Title: **Influence of the oxide thickness of a SiO_2/Si(001) substrate on the optical second harmonic intensity of few-layer $MoSe_2$**

Yoshihiro Miyauchi[1], Ryo Morishita[2], Masatoshi Tanaka[2], Sinya Ohno[2], Goro Mizutani[3], and Takanori Suzuki[1,2]*

[1]Department of Applied Physics, National Defense Academy of Japan, Yokosuka, Kanagawa 239-8686, Japan
[2]Graduate School of Engineering, Yokohama National University, Yokohama 240-8501, Japan
[3]School of Materials Science, Japan Advanced Institute of Science and Technology, Nomi, Ishikawa 923-1292, Japan

*E-mail: tsuzuki@nda.ac.jp

Abstract

The nonlinear optical properties of few-layer $MoSe_2$ on a SiO_2/Si substrate were investigated with our optical second harmonic generation (SHG) microscope. Few-layer flakes were mechanically exfoliated from a single crystal onto a 90- or 270-nm-thick SiO_2-coated Si(001) substrate. The polar plot of the second-harmonic (SH) intensity from a mono- or trilayer $MoSe_2$ flake as a function of the rotation angle of incident polarization shows a threefold symmetry, indicating that the isolated few-layer flakes retain their single crystallographic orientation. SHG spectra were found to depend strongly on the oxide thickness of the substrate (90 or 270 nm), which was interpreted using the interference among the multiply reflected SH light beams in the system. By taking this interference into account, a resonant peak may be identified at a two-photon energy of equal to or less than 2.9 eV in an SHG spectrum. The spatial resolution of the SHG microscope was estimated as 0.53 μm.

1. Introduction

The family of monolayer transition-metal dichalcogenides TX_2 (T = Mo, W; X = S, Se) has attracted much attention because monolayer TX_2 could complement graphene in various applications that require thin, transparent semiconductors, such as optoelectronics [1-4]. These materials are direct-band-gap semiconductors that possess very different properties from graphene; monolayer MoS_2 transistors with a hafnium oxide dielectric gate showed a room-temperature single-layer MoS_2 mobility of up to 200 $cm^2\ V^{-1}\ s^{-1}$, similar to that of graphene nanoribbons, current on/off ratios of 10^8, and ultralow standby power dissipation [4].

The linear optical properties of monolayer dichalcogenides have shown a marked increase in photoluminescence efficiency arising from the direct gap [5-7], where dielectric functions were obtained by the Kramers-Krönig constrained analysis of the reflectance spectra of monolayer TX_2 [8]. A laser system based on monolayer WS_2 was also demonstrated by harnessing the unique advantages of atomically thin crystals for coherent light generation [9].

The nonlinear optical properties of mono- and few-layer dichalcogenides have also been well investigated; in particular, optical second-harmonic generation (SHG) microscopy has become an indispensable tool for investigating electronic and nonlinear optical properties of few-layer TX_2, WS_2 [10-13,18], WSe_2 [10,13-15], MoS_2 [2, 3, 13, 16-18], and $MoSe_2$ [13, 19, 20]. The wavelength dependence of the SH intensity from mono- or few-layer TX_2 on a thick thermal oxide-coated Si substrate was also reported [2,11-13,15, 19, 20].

The layer number of a thin film is usually identified by the well-established procedure utilizing the optical contrast among the reflected beams in the thin film demonstrated for a 300-nm-thick SiO_2-coated Si substrate [21]. Graphene crystallites prepared on Si wafers with a certain SiO_2 thickness are visualized by optical microscopy based on the Fresnel law modeling of normal light incidence from air (refractive index n_0 = 1) onto a trilayer structure consisting of graphene, SiO_2, and Si [21]. The visual contrast sensitively depends on the SiO_2 thickness, light wavelength, and the thickness of graphene crystallites [21].

An anomaly in the G-band Raman intensity of graphene sheets on a 300-nm-thick SiO_2/Si substrate is explained by the interference effect of multiply reflected Raman light inside the graphene layer [22]. The strain-induced SHG intensity from a SiO_2/Si(111) interface was shown to change markedly as a function of oxide thickness ranging from 2 to 300 nm, owing to multiple reflections in the oxide film [23].

The SH spectra of few-layer TX_2 on a SiO_2/Si substrate are also likely to reflect the interference of multiple reflections. Thus, the interference effect must be carefully examined in the case of the wavelength dependence of SH light generated at few-layer $MoSe_2$ on a thick thermal oxide-coated Si substrate [13,19,20].

In this study, we demonstrated that the wavelength dependence of the SHG intensity from mono- or few-layer $MoSe_2$ on a 90- or 270-nm-thick SiO_2-coated Si(001) substrate crucially reflects the interference among the multiply reflected fundamental and SHG light beams in SiO_2 films. The SHG intensity increased steeply with the decrease in two-photon energy in the case of 270-nm-thick oxides, whereas there was a peak at a two-photon energy of equal to or less than 2.9 eV in the spectra in the case of 90-nm-thick oxides. Hereafter, we call the peak a peak at $\leq$2.9 eV. We followed the calculation method [22] by simply replacing the Raman light with the SHG light to take the interference effect into account in obtaining our SHG spectra. For monolayer $MoSe_2$ at an oxide thickness of 270 nm, a very low SHG intensity is expected at around 3.1 eV owing to a destructive interference. For monolayer $MoSe_2$ at an oxide thickness of 90 nm, the SHG intensity is determined to be less affected by the interference effects for the photon energy range studied, revealing a peak at $\leq$2.9 eV in the SHG spectra.

Yin et al. observed one-dimensional nonlinear optical edge states of a single atomic membrane of MoS_2 [18]. To accurately investigate the electronic states at the edges, the microscope used is required to have a sufficient spatial resolution, which is yet to be obtained. Here, we estimated the spatial resolution of our SHG microscope to be 0.53 μm.

2. Experimental procedure

Mono- and few-layer $MoSe_2$ flakes were mechanically exfoliated from a single crystal onto a SiO_2 / Si(001) substrate. The crystal was grown by Br_2 vapor transport [24]. We used a 90- or 270-nm-thick SiO_2-coated Si(001) substrate. The layer number of a $MoSe_2$ flake was identified by atomic force microscopy (AFM; Bruker Innova). For the SHG measurements, the fundamental pulse from a Ti-sapphire oscillator (Spectra Physics Mai Tai, pulse duration 80 fs, wavelength 740–880 nm, repetition rate 80 MHz, power 900 mW, mode quality M^2 <1.1, beam divergence <1.2 mrad, beam diameter <1.2 mm) was guided through a Faraday isolator, a polarizer, and a low-pass filter, and then was reflected by a dielectric multilayer mirror in an Nikon optical microscope (Nikon Y-FL). The light beam was then focused by an objective lens (Nikon LU plan ×100, numerical aperture 0.9, focal length 2 mm) onto the sample at normal incidence. The light at the double frequency generated by the sample was allowed to pass through the objective lens,

the dielectric multilayer mirror, a high-pass filter, a polarizer, and a monochromator, and was finally detected by a photomultiplier tube. We obtained the SHG microscopy image by raster scanning the target position by controlling an automated X-Y stage (Sankei SAS-2V-XYF) with a minimum step size of 0.1 μm. We monitored the pulse durations of tunable fundamental light by using a spectrum analyzer (Ocean Photonics LSM-min) during the experiment. Varying the path length through the prisms inside the laser cavity, we control the amount of dispersion at each wavelength in order to keep the laser bandwidth at a fixed value.

3. Results and discussion

Figure 1(a) shows an optical microscopy image of a few-layer $MoSe_2$ flake on a SiO_2 (270 nm) / Si(001) substrate. The mono-, bi-, and trilayer regions are marked. Figure 1(b) shows the SHG image collected from the $MoSe_2$ flake shown in Fig. 1(a). The SHG showed well-defined odd-even layer regions, which reproduced the previous results [2]. A strong SHG signal was observed from the monolayer and trilayer, whereas the signal disappeared in the bilayer region. This observation is usually explained by the symmetry of the crystals as follows. A bulk $MoSe_2$ crystal with 2*H* stacking order belongs to the space group D_{6h}, which is inversion-symmetric. Thus, its second-order nonlinear response should vanish [25]. The inversion symmetry is broken in a monolayer with D_{3h} symmetry. However, in a bilayer with the space group D_{3d}, the inversion symmetry is present again. In general, an even number of layers belong to the D_{3d} point group, and an odd number of layers belong to the D_{3h} point group [2, 16].

Figure 2 shows the intensity profile of the SH light obtained by scanning the irradiated position from left to right along the dotted line in Fig. 1(a). From this profile, the SHG intensity from the monolayer was about twice as high as that from the trilayer, whereas the intensity from the bilayer was almost three orders of magnitude lower than that from the monolayer.

A schematic of the lattice structure of monolayer $MoSe_2$ is shown in Fig. 3(a). For the odd layer with D_{3h} point-group symmetry, the nonvanishing second-order susceptibility tensors are $\chi^{(2)}_{xxx} = -\chi^{(2)}_{xyy} = -\chi^{(2)}_{yxy} = -\chi^{(2)}_{yyx}$, where *x* and *y* are along the armchair and zigzag directions shown in Fig. 3(a), respectively [25]. SHG intensity as a function of the sample angle for a pump laser polarization parallel to the analyzer may be expressed as $I \propto \cos^2(3\phi + \phi_0)$, where ϕ is the angle between the input laser polarization and the x-direction, and ϕ_0 is the initial crystallographic orientation of the $MoSe_2$ sample [2]. Figure 3(b) shows polar plots of the SHG intensity from a monolayer

$MoSe_2$ flake as a function of the sample angle. The pattern clearly shows that the sample has a threefold rotational symmetry. Because the measurement is direction-insensitive, there is an arbitrariness of 60° in the definition of the x-axis. According to the plot, $\phi_0 \sim$ -10° indicates the offset angle for setting the armchair (x) direction of $MoSe_2$ with respect to the input laser polarization.

Figure 3(c) shows the polar plots of the SHG intensity as a function of the sample angle from a trilayer $MoSe_2$ flake that lies next to the monolayer flake. The pattern of the SHG intensity from the trilayer has the same dependence on the sample angle as that from the monolayer in Fig. 3(a). This observation indicates that the few-layer $MoSe_2$ flakes that mechanically exfoliated from a sample retained the crystallographic structure of the layers in the bulk crystal.

Figures 4(a) and 4(b) show the wavelength dependence of the SH intensity for monolayer $MoSe_2$ on 270- and 90-nm-thick SiO_2-coated Si(001) substrates obtained with a fixed laser power of 0.5 mW without the polarizer for the SH light, respectively. The SHG spectra are normalized by a crystalline quartz reference placed at the sample position. The SH intensity corresponds to the $\chi^{(2)}_{xxx}$ tensor element [25]. The SHG intensity increases steeply with the decrease in two-photon energy in Fig. 4(a), whereas a peak at $\leq$2.9 eV is observed in the spectra in Fig. 4(b). The spectra of the $MoSe_2$ monolayer depending strongly on the oxide thickness of the substrate might be interpreted using the interference among the multiply reflected fundamental and SH light beams in the system. The strain-induced SH intensity at the SiO_2 / Si(111) interface was shown to change markedly as a function of oxide thickness, owing to multiple reflections in the oxide film [23]. The strain-induced SH intensity from our bare 90-nm-thick SiO_2-coated Si(001) substrate, however, may be expected to be low owing to the fourfold symmetry of the Si(001) interface where SHG is forbidden at normal incidence. Actually, it was almost of the fifth order of magnitude lower than that from monolayer $MoSe_2$ on the SiO_2/Si substrate.

Wang et al. [22] observed an unusually high G-band Raman intensity for monolayer graphene on a Si substrate with a 300 nm SiO_2 capping layer, and they explained their results by considering the multiple reflections of both the Raman light and the incident light in the graphene layer. We followed their calculation method [22] by simply replacing the Raman light with the SH light, and simulated the interference among the multiply reflected fundamental and SH light beams in the systems by using the optical constant of bulk $MoSe_2$ [26]. For monolayer $MoSe_2$ at an oxide thickness of 270 nm [Fig. 4(a)], the steep minimum intensity at around 3.1 eV and the increase in SHG intensity

towards a low photon energy are qualitatively reproduced (see supplementary data at http://stacks.iop.org/JJAP/55/085801/mmedia). For monolayer $MoSe_2$ at an oxide thickness of 90 nm, on the other hand, the calculation shows that the interference effects are less important for the photon energy range studied, and thus the raw SHG spectra in Fig. 4(b) would be sufficiently close to the unaffected SHG spectra. Therefore, the peak position at ≤2.9 eV identified in the SHG spectra in Fig. 4(b) may show the resonance enhancement in the electronic states of monolayer $MoSe_2$.

The SH intensity reported for monolayer $MoSe_2$ on a 285-nm-thick SiO_2 / Si substrate [20] showed a minimum intensity at ~1.45 eV or its second harmonics at ~2.9 eV, which is clearly different from the minimum intensity at ~3.1 eV for our 270-nm-thick SiO_2 / Si substrate. The energy for the minimum SH intensity reflecting the interference of the multiply reflected SH light beams may be inversely proportional to the oxide thickness [22, 27]. Thus, the thickness ratio of the two SiO_2 / Si substrates applied to monolayer $MoSe_2$ at an oxide thickness of 285 nm would give a minimum intensity of about 2.9 eV. Then, the minimum at ~1.45 eV in Fig. 2 of Ref. 21 is likely to reflect this interference.

The dielectric function of $MoSe_2$ monolayers for photon energies from 1.5 to 3 eV was obtained by Li et al. from the reflection spectra by Kramers-Krönig constrained vibrational analysis [8]. They obtained the peaks labeled A and B in the photon energy range of 1.5–2 eV, which correspond to excitons from the two spin-orbit split transitions at the K point of the Brillouin zone. They also observed that the resonance energies labeled C and D peaks above 2 eV are modestly shifted from that of the corresponding bulk material, which has a very sharp strong peak near 3 eV and a somewhat weaker, although equally sharp structure near 4–5 eV for bulk $MoSe_2$ [26]. The C and D features are discussed to be associated with transitions away from the K point and involve a significant contribution from chalcogen orbitals [8].

The peak corresponding to the one-photon resonance with the A exciton transition may be expected at around 3.2 eV in Fig. 4(b); however, this is clearly not the case. The resonance may be attributed to the two-photon resonance with the C interband transition, which is reasonably expected above 2.5 eV [8]. Thus, we may conclude that the peak at ≤2.9 eV in the SHG spectra arises from the two-photon resonance with the C interband transition. Further identification of SHG resonance would require a detailed experimental study with a laser system having an extended wavelength tuning range.

The resolution of the SHG microscope was also estimated using a 16 –84% criterion corresponding to twice the root mean square (RMS) width of a Gaussian function when convoluted with a step function [28]. By analyzing the steepness of the

intensity profile obtained by scanning the irradiated position with a step size of 0.2 μm as shown in the inset of Fig. 2, we estimated the resolution as 0.53 μm. In the case of an ideal Gaussian-shaped beam (M^2 ~1), the theoretical beam diameter at the focal point is estimated by $4\lambda f / \pi w_e$ [29], where λ and f are the wavelength and focal length, respectively. w_e is the laser beam diameter at the objective lens estimated as 3.4 mm. In our system, λ = 800 nm and f = 2 mm indicate the beam diameter at the focal point to be 0.60 μm. For SHG, the spatial distribution of SHG intensity may be proportional to the square of the Gaussian as

$$\exp^2(-\frac{x^2}{2\sigma^2}) = \exp(-\frac{x^2}{2(\sigma/\sqrt{2})^2}),$$

where x is the position of the beam profile and σ is the RMS width of the Gaussian distribution. Thus, the theoretical spatial resolution of the SHG microscope is obtained as 0.60 μm /√2 = 0.42 μm by dividing the beam diameter at the focal point by √2. The spatial resolution of our SHG microscope of 0.53 μm is sufficiently close to the theoretical spatial resolution.

4. Conclusions

We developed an SHG microscope and measured the SHG intensity from few-layer $MoSe_2$ on a 90 - or 270-nm-thick SiO_2 / Si(001) substrate as a function of the layer number, sample angle, and incident wavelength. The SHG microscopy images and intensity profile show that the SHG intensity from monolayer $MoSe_2$ was twice as high as that from trilayer $MoSe_2$, whereas the intensity from the bilayer was less than three orders of magnitude lower than that of the monolayer. The sample angle dependence shows that the mechanically exfoliated few-layer $MoSe_2$ flakes retained the crystallographic structure of the layers in a bulk crystal. SHG spectra of the monolayer $MoSe_2$ depended strongly on the oxide thickness of the substrate, which was interpreted using the interference among the multiply reflected SH light beams in the system. A resonant peak may be identified at a two-photon energy of equal to or less than 2.9 eV in an SHG spectrum. The spatial resolution of the SHG microscope was estimated as 0.53 μm from the intensity profile.

References

[1] A. K. Geim and I. V. Grigorieva, Nature **499**, 419 (2013).

[2] L. M. Malard, T. V. Alencar, A. P. M. Barboza, K. F. Mak, and A. M. Paula, Phys. Rev. B **87**, 201401 (2013).

[3] C. Lee, G. Lee, A. M. Zande, W. Chen, Y. Li, M. Han, X. Cui, G. Arefe, C. Nuckolls, T. F. Heinz, J. Guo, J. Hone, and P. Kim, Nat. Nanotechnol. **9**, 676 (2014).

[4] B. Radisavljevi, A. Radenovic, J. Brivio, V. Giacometti, and A. Kis, Nat. Nanotechnol. **147**, (2011).

[5] A. Splendiani, L. Sun, Y. Zhang, T. Li, J. Kim, C. Y. Chim, G. Galli, and F. Wang, Nano Lett. **10**, *1271* (2010).

[6] G. Kioseoglou, A. T. Hanbicki, M. Currie, A. L. Friedman, D. Gunlycke and B. T. Jonker, Appl. Phys. Lett. **101**, 221907(2012).

[7] W. Zhao, Z. Ghorannevis, L. Chu, M. Toh, C. Kloc, P. H. Tan and G. Eda, ACS Nano **7**, 791(2013).

[8] Y. Li, A. Chernikov, X. Zhang, A. Rigosi, H. M. Hill, A. M. Zande, D. A. Chenet, E. Shih, J. Hone, and T. F. Heinz, Phys. Rev. B **90**, 205422 (2014).

[9] S. Wu, S. Buckley, J. R. Schaibley, L. Feng, J. Yan, D. G. Mandrus, F. Hatami, W. Yao, J. Vucovic, A. Majumdar, and X. Xu, Nature. **520**, 69 (2015).

[10] H. Zeng, G. Liu, J. Dai, Y. Yan, B. Zhu, R. He, L. Xie, S. Xu, X. Chen, W. Yao and X. Cui, Sci. Rep. **3**, 1608 (2013).

[11] C. Janisch, Y. Wang, D. Ma, N. Mehta, A. L. Elias, N. P. Lopez, M. Terrones, V. Crespi, and Z. Liu, Sci. Rep. **4**, 5530 (2014).

[12] Z. Ye, T. Cao, K. O'Brien, H. Zhu, X. Yin, S. G. Louie, and X. Zhang, Nature **513**, 214 (2014).

[13] X. Zhang, C. Lin, Y. Tseng, K. Huang, and Y. Lee, Nano Lett. 15, 410 (2015).

[14] K. He, N. Kumar, L. Zhao, Z. Wang, K. F. Mak, H. Zhao, and J. Shan, Phys. Rev. Lett. **113**, 026803 (2014).

[15] G. Wang, X. Marie, I. Gerber, T. Amand, D. Lagarde, L. Bouet, M. Vidal, A. Balocchi, and B. Urbaszek, Phys. Rev. Lett. **114**, 097403 (2015).

[16] N. Kumar, S. Najmaei, Q. Cui, F. Ceballos, P. M. Ajayan, J. Lou, and H. Zhao, Phys. Rev. B **87** 161403 (2013).

[17] W. Wu, L. Wang, Y. Li, F. Zhang, L. Lin, S. Niu, D. Chenet, X. Zhang, Y. Hao, T. F. Heinz, J. Hone and Z. L. Wang, Nature **514**, 470 (2014).

[18] X. Yin, Z Ye, D. A. Chenet, Y. Ye, K. O'Brien, J. C. Hone, and X. Zhang, Science **344**, 488 (2014).

[19] G. Wang, I. C. Gerber, L. Bouet, D. Lagarde, A. Blocchi, M. Vidal, E. Palleau, T. Amand, X. Marie, and B. Urbaszek, 2D Mater. **2**, 045005 (2015).
[20] D. H. Kim and D. Lim, J. Korean Phys. Soc. **66**, 816 (2015).
[21] P. Blake, E. W. Hill, A. G. C. Betim S. Novoselov, D. Jiang, R. Yang, T. J. Booth, and A. K. Geim, Appl. Phys. Lett. **91**, 063124 (2007).
[22] Y. Y. Wang, Z. H. Ni, Z. X. Shen, H. M. Wang, and Y. H. Wu, Appl. Phys. Lett. **92**, 043121 (2008).
[23] C. W. van Hasselt, M. A. C. Devillers, Th. Rasing, and O. A. Aktsipetrov, J. Opt. Soc. Am. B **33**, 12 (1995).
[24] M. Tanaka, H. Fukutani, and G. Kuwabara, J. Phys. Soc. Jpn. 45, 1899 (1978).
[25] Y. R. Shen, *The Principles of Nonlinear Optics* (Wiley, Hoboken, NJ, 2003) p. 27.
[26] A. R. Beal and H. P. Hughes, Solid State Phys. **12**, 881 (1979).
[27] M. Born and E. Wolf, *Principles of Optics* (Wiley, New York, 1984) p. 352.
[28] D. Berger and J. Nissen, Mater. Sci. Eng. **55**, 012002 (2014).
[29] J. D. Winefordner, *Raman Spectroscopy for Chemical Analsis* (Wiley, New York, 2000) p. 295.

Figure Captions

Fig. 1. (a) Optical microscopy image of a $MoSe_2$ thin film on a SiO_2 (270 nm) / Si(001) substrate. By measuring the height relative to the substrate by AFM, $MoSe_2$ was determined as monolayer (1L), bilayer (2L), and trilayer (3L). The scale bar is 5 μm. (b) Topographical representation of the SHG image obtained for the $MoSe_2$ flake in (a).

Fig. 2. Intensity profile of the SH light scanned from left to right along the dotted line in Fig. 1(a). The inset shows the intensity profile fitted by a step function of the scanned SH light obtained with a step size of 0.2 μm.

Fig. 3. (a) Lattice structure of monolayer $MoSe_2$. Polar plots of the SH intensity for (b) mono- and (c) trilayer $MoSe_2$ as a function of the sample angle. The solid curves serve as visual guides.

Fig. 4. SHG spectra of monolayer $MoSe_2$ on (a) 270- and (b) 90-nm-thick SiO_2-coated Si(001) substrates. The solid curve serves as a visual guide. The SHG spectra are normalized by a crystalline quartz reference placed at the sample position.

Figures

Figure 1

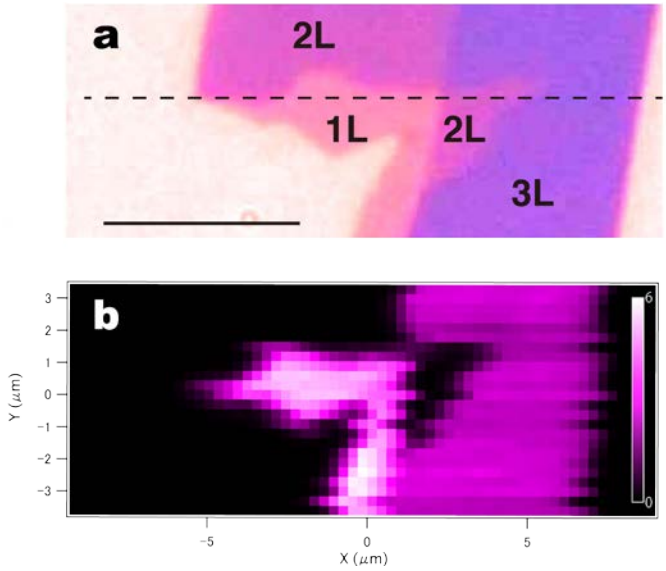

Figure 2

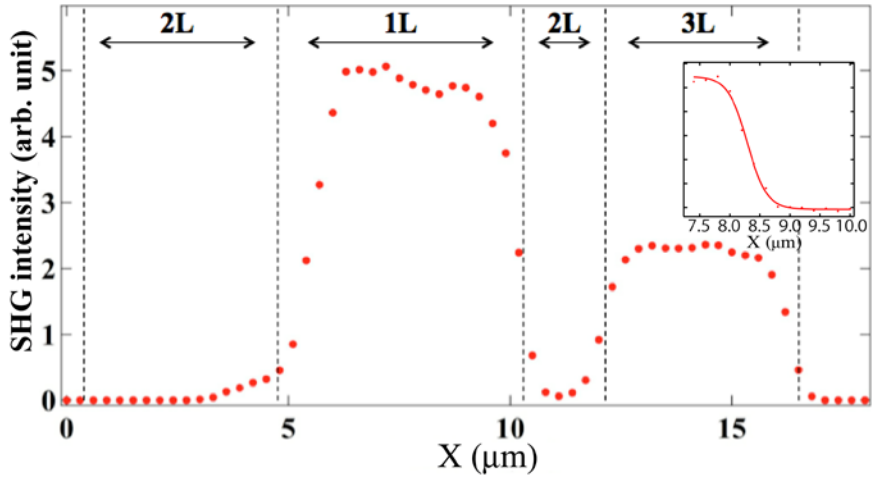

Figure 3

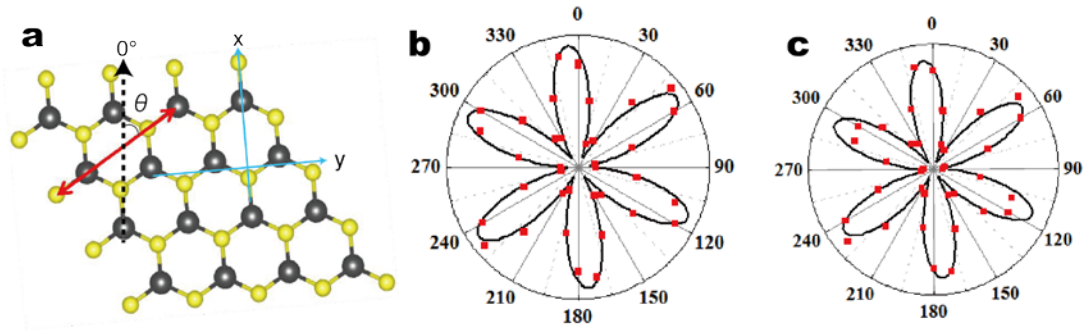

Figure 4